RESEARCH ARTICLE

EcoMat
FUNCTIONAL MATERIALS FOR GREEN ENERGY AND ENVIRONMENT

WILEY

Achieving an excellent efficiency of 11.57% in a polymer solar cell submodule with a 55 cm^2 active area using 1D/2A terpolymers and environmentally friendly nonhalogenated solvents

Hyeonwoo Jung[1] | Jongyoun Kim[1] | Jaehyoung Park[1] |
Muhammad Jahankhan[2] | Youngjun Hwang[1] | Byeongjae Kang[1] |
Hyerin Kim[3] | Ho-Yeol Park[3] | Pyeongkang Ahn[4] | DuHyeon Um[5] |
Je-Sung Jee[3] | Won Suk Shin[2] | BongSoo Kim[4,5,6] | Sung-Ho Jin[3] |
Chang Eun Song[2] | Youngu Lee[1]

[1]Department of Energy Science and Engineering, DGIST, Daegu, Republic of Korea

[2]Advanced Energy Materials Research Center, Korea Research Institute of Chemical Technology (KRICT), Daejeon, Republic of Korea

[3]Department of Chemistry Education, Graduate Department of Chemical Materials, Institute for Plastic Information and Energy Materials, Sustainable Utilization of Photovoltaic Energy Research Center (ERC), Pusan National University, Busan, Republic of Korea

[4]Department of Chemistry, Ulsan National Institute of Science and Technology (UNIST), Ulsan, Republic of Korea

[5]Graduate School of Semiconductor Materials and Device Engineering, Ulsan National Institute of Science and Technology (UNIST), Ulsan, Republic of Korea

[6]Graduate School of Carbon Neutrality, Ulsan National Institute of Science and Technology (UNIST), Ulsan, Republic of Korea

Correspondence
Sung-Ho Jin, Department of Chemistry Education, Graduate Department of Chemical Materials, Institute for Plastic Information and Energy Materials, Sustainable Utilization of Photovoltaic Energy Research Center (ERC), Pusan National University, Busan 46241, Republic of Korea.
Email: shjin@pnu.ac.kr

Chang Eun Song, Advanced Energy Materials Research Center, Korea Research Institute of Chemical Technology (KRICT), 141 Gajeong-ro, Yuseong, Daejeon, 34114, Republic of Korea.
Email: songce@krict.re.kr

Youngu Lee, Department of Energy Science and Engineering, DGIST, 333, Techno Jungang-daero, Hyeonpung-eup, Dalseong-gun, Daegu, 42988,

Abstract

The transition of polymer solar cells (PSCs) from laboratory-scale unit cells to industrial-scale modules requires the development of new p-type polymers for high-performance large-area PSC modules based on environmentally friendly processes. Herein, a series of 1D/2A terpolymers (PBTPttBD) composed of benzo[1,2-*b*:4,5-*b'*]dithiophene (BDT-F), thieno[3,4-*c*]pyrrole-4,6(5*H*)-dione (TPD-TT), and benzo-[1,2-*c*:4,5-*c'*]dithiophene-4,8-dione (BDD) is synthesized for nonhalogenated solvent processed PSC submodules. The optical, electrochemical, charge-transport, and nano-morphological properties of the PBTPttBD terpolymers are modulated by adjusting the molar ratio of the TPD-TT and BDD components. PBTPttBD-75:BTP-eC11-based PSC submodules, processed with *o*-xylene, achieve a notable PCE of 11.57% over a 55 cm^2 active area. This PCE value is among the highest reported using a nonhalogenated solvent over a 55 cm^2 active area module. The optimized PSC submodule exhibits minimal cell-to-module loss, which can be attributed to the optimized

Republic of Korea.
Email: youngulee@dgist.ac.kr

crystallinity of the PBTPttBD-75:BTP-eC11 photoactive layer system and favorable film formation kinetics.

1 | INTRODUCTION

Polymer solar cells (PSCs) employing a bulk heterojunction structure exhibit a significant potential as energy sources for advanced portable electronic devices due to their low weight, excellent flexibility, scalable roll-to-roll (R2R) processing, cost-effectiveness, and semitransparency.[1–5] Recent advances in the design of high-performance photoactive materials and device structure optimization, have resulted in a remarkable increase in the power conversion efficiency (PCE) of PSCs, surpassing 19%.[6,7] However, most research efforts have been primarily focused on achieving high efficiency in small-area unit cells, which are typically fabricated using spin-coating techniques.[8–10] To facilitate the transition of PSCs from laboratory-scale unit cells to industrial-scale modules, it is crucial to advance efficient technologies that enable the expansion of the active area of devices while minimizing the performance loss and ensuring operational stability.[11–13] In contrast to spin-coating method, large-scale coating methods such as bar-coating, blade-coating, and slot-die coating lead to prolonged solvent evaporation time, especially in high-boiling-point solvent systems. The extended film formation process can cause excessive molecular aggregation, leading to severe phase separation between the polymer and non-fullerene acceptor, which results in poor device performance.[14–16]

Recently, the PM6 polymer, which employs an alternating electron donor-electron acceptor (D-A) structure has been widely used in the photoactive layers of PSCs due to its high crystallinity, superior hole mobility, and strong pre-aggregation behavior.[17-19] However, achieving high-performance PSCs based on the PM6 polymer normally requires the use of halogenated solvents, such as chloroform (CF) and chlorobenzene (CB). These solvents are employed to ensure sufficient solubility and favorable molecular ordering. Unfortunately, the use of these halogenated solvents is limited in mass production because of environmental toxicity concerns.[20-27] Furthermore, due to the strong temperature dependent aggregation (TDA) property of the PM6 polymer, PM6-based large-area PSCs fabricated using large-scale coating methods exhibit a significant reduction in PCE. For example, PM6-based small-area (0.12 cm^2) PSCs exhibit a PCE of 15.1%.

However, the PCE of PM6-based large-area (54.5 cm^2) PSC submodules can be significantly reduced to 8.73%.[28] This decrease in performance of PM6-based large-area PSCs in nonhalogenated systems can be attributed to the oversized domains and nonuniformity in the photoactive layer, leading to an increased cell-to-module (CTM) loss. The undesirable morphology of the PM6-based photoactive layer can be controlled using a high-temperature (HT) process such as a hot solution and/or preheated substrates (70 ∼ 160°C).[15,29] However, such a complicated process is unsuitable for the production of cost effective and highly reproducible R2R PSC modules. Therefore, it is necessary to develop new p-type polymer for high-performance large-area PSC modules based on simple processes and minimize the CTM loss in nonhalogenated systems.

Terpolymers composed of three different monomers have recently attracted attention as promising p-type polymer. Terpolymers can accurately control physicochemical properties, such as frontier energy levels, light harvesting ability, pre-aggregation behavior, miscibility, and crystallinity, by introducing a third component directly into the donor-acceptor (D-A) copolymer backbone.[30–32] Despite their advantages, the performance of terpolymer-based large-area PSCs still lags behind that of copolymer-based large-area PSCs. In addition, few studies on high-performance large-area PSC modules using nonhalogenated solvents have been reported in the literature.

Herein, we synthesize a new series of 1D/2A terpolymers for developing room-temperature (RT) and nonhalogenated solvent processed high-performance PSCs submodules. The terpolymers are composed of three components: benzo[1,2-*b*:4,5-*b'*]dithiophene (BDT-F), thieno[3,4-*c*]pyrrole-4,6(5*H*)-dione (TPD-TT), and benzo-[1,2-*c*:4,5-*c'*]dithiophene-4,8-dione (BDD). Three PBTPttBD terpolymers (i.e., PBTPttBD-25, PBTPttBD-50, and PBTPttBD-75) are synthesized using different ratios TPD-TT to BDD composition ratios, corresponding to TPD-TT contents of 25%, 50%, and 75%, respectively. The composition ratio of the TPD-TT and BDD components can be used to control the light harvesting ability, energy level, molecular ordering, and charge transport properties of the PBTPttBD polymers. A grazing incidence wide-angle x-ray

scattering and contact angle analysis show that the PBTPttBD-75:BTP-C11 blended film exhibits a predominant face-on orientation with good miscibility. The RT and non-halogenated solvent processed PBTPttBD-75:BTP-eC11 PSC exhibits a high PCE of 15.55%. Furthermore, PBTPttBD-75: BTP-eC11-based PSC submodules, processed with *o*-xylene under RT conditions, achieve a notable PCE of 11.57% over a 55 cm^2 active area. This PCE value is among the highest reported in single-junction PSC submodules processed with nonhalogenated solvent.

2 | RESULTS AND DISCUSSIONS

2.1 | Material synthesis and thermal stability

We designed novel PBTPttBD terpolymers, consisting of one electron-donor component (BDT-F) and two electron-acceptor components (TPD-TT and BDD), as shown in Figure 1. Three terpolymers, PBTPttBD-25, PBTPttBD-50, and PBTPttBD-75, were synthesized by employing the palladium-catalyzed Stille polymerization, where different molar ratios of the electron-acceptor components (TPD-TT and BDD) were used. For comparison, copolymers, PM6 and PBTPttBD-100 were also prepared. After polymerization, sequential Soxhlet extraction was performed with methanol, acetone, *n*-hexane, and dichloromethane to purify the polymers. In contrast to the PM6 polymer, PBTPTTBD-25, PBTPttBD-50, PBTPttBD-75, and PBTPttBD-100 exhibited good solubility in nonhalogenated solvents, such as toluene, *o*-xylene, and tetrahydrofuran. By incorporating thieno[3,2-*b*]thiophene as a π-bridge in the TPD-TT component, the light absorption and hole mobility were improved due to the extended conjugation length. Additionally, by introducing steric hindrance between the polymer chains, the bulky alkyl chains of the TPD-TT component could effectively control the crystallinity and aggregation behavior of the PM6 polymer backbone. Also, the introduction of the TPD-TT component into the PM6 polymer backbone was expected to decrease the structural order within the polymer backbone, thus reducing the aggregation behavior in nonhalogenated solvents. Furthermore, the quinoid structure of the TPD-TT component was expected to reduce the highest occupied molecular orbital (HOMO) energy level, potentially leading to high open-circuit voltage (V_{oc}) values.[33–36]

To determine the molecular characteristics of the polymers, we measured the number-average molecular weight (M_n), weight-average molecular weight (M_w), and polydispersity index (PDI) of all polymers by employing HT gel permeation chromatography with *o*-DCB as the eluent at 80°C, calibrated using polystyrene. The measured M_n values of PM6, PBTPttBD-25, PBTPttBD-50, PBTPttBD-75, and PBTPttBD-100 were 27.1, 31.7, 45.0, 48.9, and 41.2 kDa, respectively, and the measured PDI values were 4.19, 4.73, 4.59, 3.97, and 4.25 respectively. Furthermore, we evaluated the thermal properties of the PM6 and PBTPttBD polymers using thermal gravimetric analysis (Figure S1). The results showed a high decomposition temperature (T_d), which exceeded 380°C, indicating that the PBTPttBD polymers exhibit excellent thermal stability, making them suitable for solar cell applications (Table 1).

2.2 | Temperature dependent absorption spectra and electrochemical properties

Figure S2 presents the normalized UV-vis absorption spectra of the polymers in diluted CB solution and thin films. These spectra exhibit two distinct absorption peaks in the 350–500 nm and 500–700 nm ranges. The first set of peaks corresponds to the π-π* transition. The second set of peaks indicates the occurrence of intramolecular charge transfer between the electron-donor and electron-acceptor components.[37–39] In the solution, the PM6 polymer exhibits a distinct shoulder peak at 581 and 619 nm, corresponding to the λ_{0-1} and λ_{0-0} transitions, respectively. On the other hand, as the content of the TPD-TT component increases in the polymer backbone, the UV–vis absorption spectra are blue-shifted, and the I_{0-0} peak gradually decreases. The optical bandgaps were 1.81 eV for PM6, 1.82 eV for PBTPttBD-25, 1.86 eV for PBTPttBD-50, 1.89 eV for PBTPttBD-75, and 1.90 eV for PBTPttBD-100. As shown in Figures S2b and S3, the three terpolymers in the film state exhibit a much more blue-shifted and broader absorption spectrum than that in the PM6 polymer, enabling increased complementary absorption with a non-fullerene acceptor (BTP-eC11). They also have a higher absorption coefficient than that in the PM6 polymer, leading to an increased short-circuit current density (J_{sc}).

To assess the impact of the TPD-TT component on the TDA property of the PM6 and PBTPttBD polymers, we analyzed their temperature-dependent absorption spectra in the 25–100°C temperature range in diluted CB solution of the PM6 and PBTPttBD polymers (Figure 2). The intensity ratio I_{0-0}/I_{0-1}, which represents the ratio between λ_{0-0} and λ_{0-1} transitions, is commonly used to evaluate the level of aggregation.[40] The PM6 polymer exhibited the highest I_{0-0}/I_{0-1} value, indicating the strongest aggregation behavior among all temperature ranges. As the content of the TPD-TT component increased, the I_{0-0}/I_{0-1} values gradually decreased, indicating a gradual
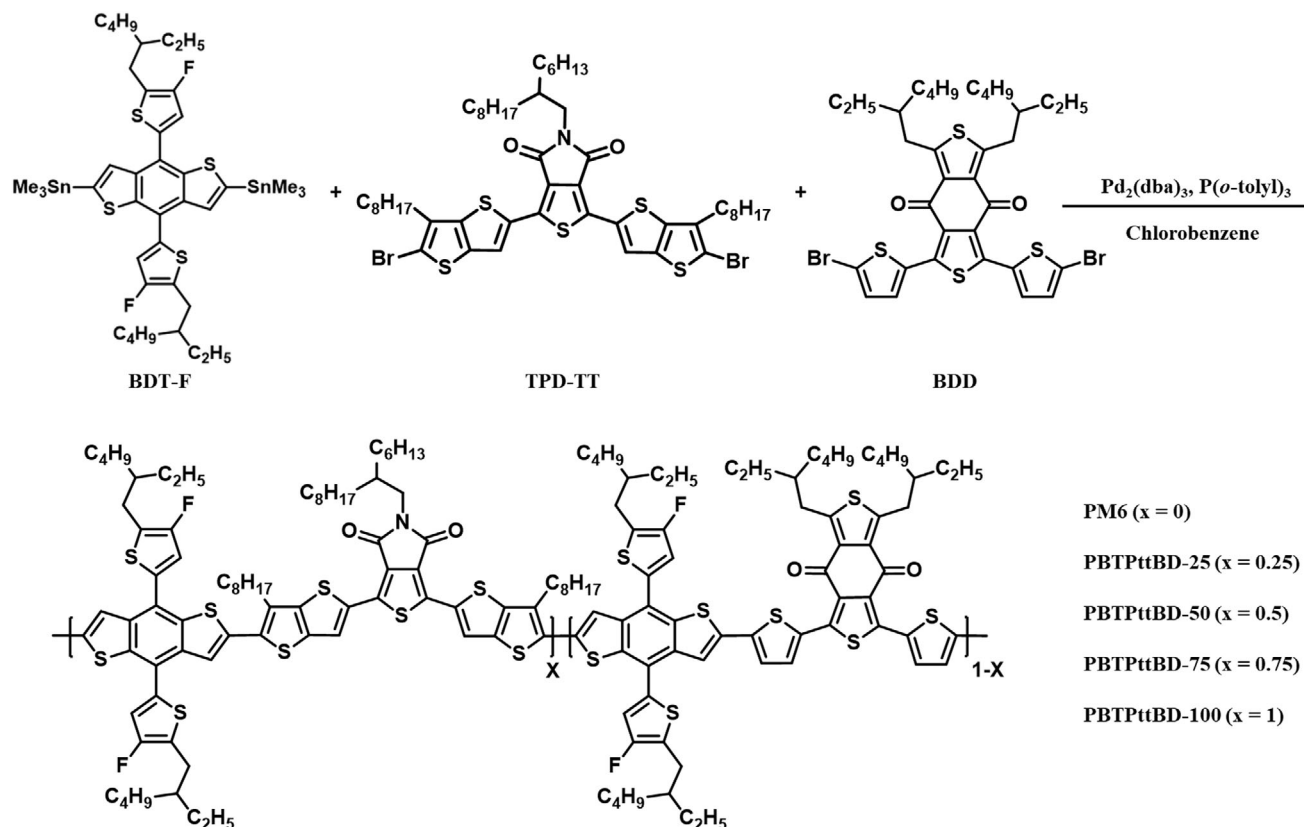
FIGURE 1 Synthesis route and structural composition of PBTPttBD polymers.

TABLE 1 Molecular characteristics and thermal stability of PM6 and PBTPttBD polymers.

Polymer	M_n [kDa]	M_w [kDa]	PDI	T_d [°C]
PM6	27.1	113.9	4.19	400
PBTPttBD-25	31.7	149.6	4.73	389
PBTPttBD-50	45.0	206.2	4.59	394
PBTPttBD-75	48.9	194.2	3.97	390
PBTPttBD-100	41.2	175.3	4.25	397

decrease in aggregation. This observation verifies that the incorporation of the TPD-TT component in the PM6 polymer backbone allows for a fine control of the polymer aggregation, leading to mild process conditions.

The electrochemical properties of the PM6 and PBTPttBD polymers were examined by conducting cyclic voltammetry (CV) measurements. The onset oxidation potentials of the PM6, PBTPttBD-25, PBTPttBD-50, PBTPttBD-75, and PBTPttBD-100 polymers were 1.16, 1.19, 1.20, 1.22, and 1.18 V, respectively (Table 2). Correspondingly, the HOMO energy levels of the PM6, PBTPttBD-25, PBTPttBD-50, PBTPttBD-75, and PBTPttBD-100 polymers were -5.52, -5.55, -5.56, -5.58, and -5.54 eV, respectively. Therefore, it is expected that the PBTPttBD-75-based-

PSCs will exhibit a V_{oc} higher than that of other polymer-based PSCs. The lowest unoccupied molecular orbital (LUMO) energy levels were determined by calculating the energy gap between the HOMO energy levels and the optical bandgaps (E_g^{opt}). The obtained values of -3.71, -3.73, -3.70, -3.69, and -3.64 eV for the PM6, PBTPttBD-25, PBTPttBD-50, PBTPttBD-75, and PBTPttBD-100 polymers, respectively, indicate that all exhibit suitable energy offsets by employing the BTP-eC11 acceptor leading to a strong driving force for exciton dissociation (Figure S4). These results show that adjusting the molar ratio of the TPD-TT and BDD components within the polymer backbone allows for a facile control over the HOMO and LUMO energy levels.

2.3 | Solar cell performance

To investigate the solar cell performance of the PM6 and PBTPttBD polymers, PSCs employing an device structure of ITO/ZnO/polymer:BTP-eC11/MoO$_3$/Ag were fabricated. The optimized solar cell performance of the PM6 and PBTPttBD polymers was obtained using _o_-xylene as a nonhalogenated solvent. A 1:1.5 polymer:BTP-eC11 blend ratio with 1,8-diiodooctane of 0.5 v/v% was used. As shown in Figure 3A, the current density-voltage (_J-V_) curves of the PM6 and PBTPttBD polymer:BTP-
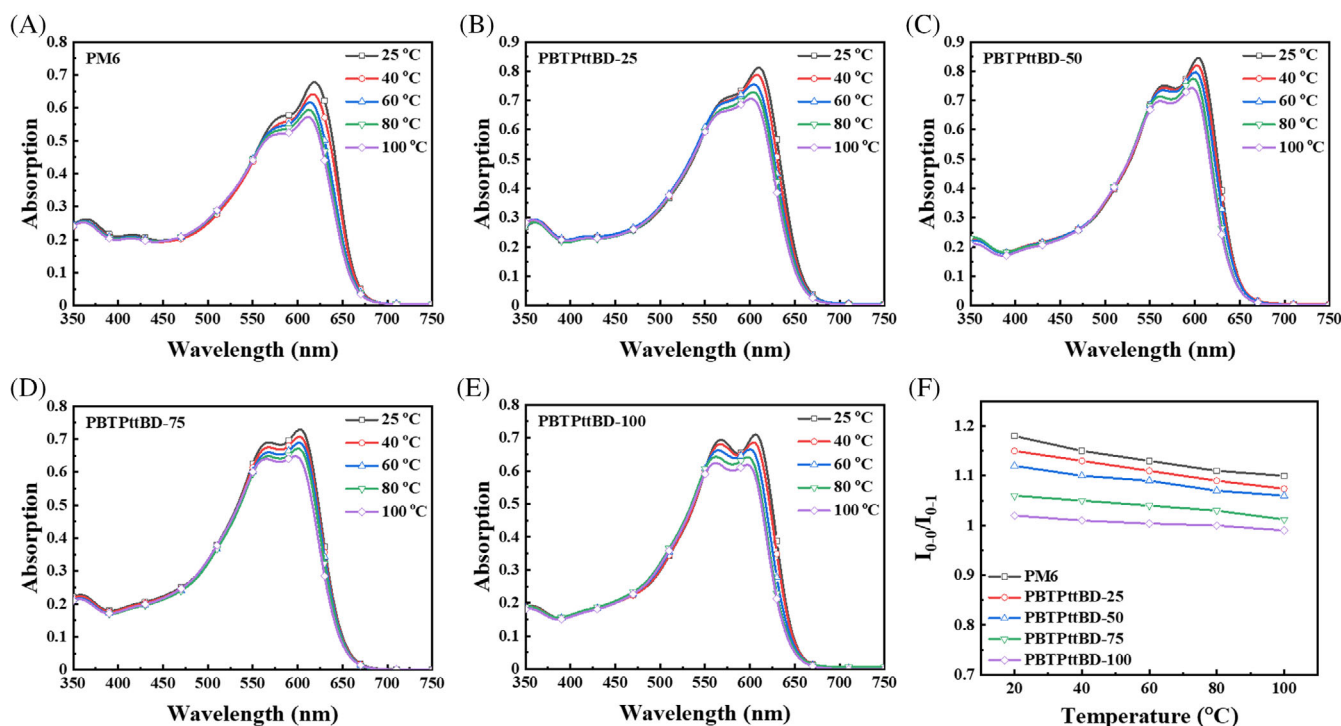
FIGURE 2 UV–vis absorption spectra of (A) PM6, (B) PBTPttBD-25, (C) PBTPttBD-50, (D) PBTPttBD-75, and (E) PBTPttBD-100 in CB solutions at various temperatures. (F) Plot of intensity ratios between I_{0-0}/I_{0-1} versus absorption dependent temperature of the PM6 and PBTPttBD polymers.

TABLE 2 Optical and electrochemical parameters of the PM6 and PBTPttBD polymers.

Polymer	$\lambda_{max,\ abs}^{sol}$ [nm]	$\lambda_{max,\ abs}^{film}$ [nm]	$E_g^{opt,a}$[eV]	E_{onset}^{ox} [V]	HOMO[b]/LUMO[c][eV]
PM6	617	623	1.81	1.16	−5.52/−3.71
PBTPttBD-25	610	609	1.82	1.19	−5.55/−3.73
PBTPttBD-50	604	607	1.86	1.20	−5.56/−3.70
PBTPttBD-75	603	607	1.89	1.22	−5.58/−3.69
PBTPttBD-100	607	565	1.90	1.18	−5.54/−3.64

[a]The E_g^{opt} was calculated using $1240/\lambda_{onset}$.
[b]Estimated from the onset oxidation potential on the CV curves.
[c]Inferred from the HOMO energy level and E_g^{opt}.

eC11-based PSCs were obtained under light irradiation of 100 mW/cm². The corresponding photovoltaic parameters of the PM6:BTP-eC11, PBTPttBD polymer:BTP-eC11-based PSCs, such as V_{oc}, J_{sc}, fill factor (FF), and PCE, are presented in Table 3. The parameter values of the RT-processed PM6:BTP-eC11-based PSCs showed a limited PCE of 13.29% with a low V_{oc} of 0.80 V, J_{sc} of 23.23 mA/cm², and FF of 71.79%, which can be attributed to undesirable film nanomorphology (Table S1). Thus, HT processing was applied to the PM6:BTP-eC11-based photoactive layer to control the film nanomorphology and the following parameter values were obtained: V_{oc} of 0.80 V, J_{sc} of 24.91 mA/cm², and FF of 75.57%, resulting in a much higher PCE of 15.05%, which is comparable to

previously reported results.[41] Since PBTPttBD-25 and PBTPttBD-50 exhibit strong TDA properties similar to the PM6 polymer, the PBTPttBD-25:BTP-eC11 and PBTPttBD-50:BTP-eC11-based PSCs were optimized using HT processing and achieved PCEs of 15.77% and 15.65%, respectively. In contrast, the PBTPttBD-75:BTP-eC11-based PSCs exhibited a slight dependence on the processing temperature conditions. Interestingly, they achieved the best efficiency of 15.55% with V_{oc} of 0.85 V, J_{sc} of 26.15 mA/cm² and FF of 70.05% under RT processing conditions. On the other hand, the PBTPttBD-100:BTP-eC11-based PSCs achieved relatively low PCE values under both HT and RT processing conditions. As a result, the PBTPttBD-75:BTP-eC11-based PSCs achieved
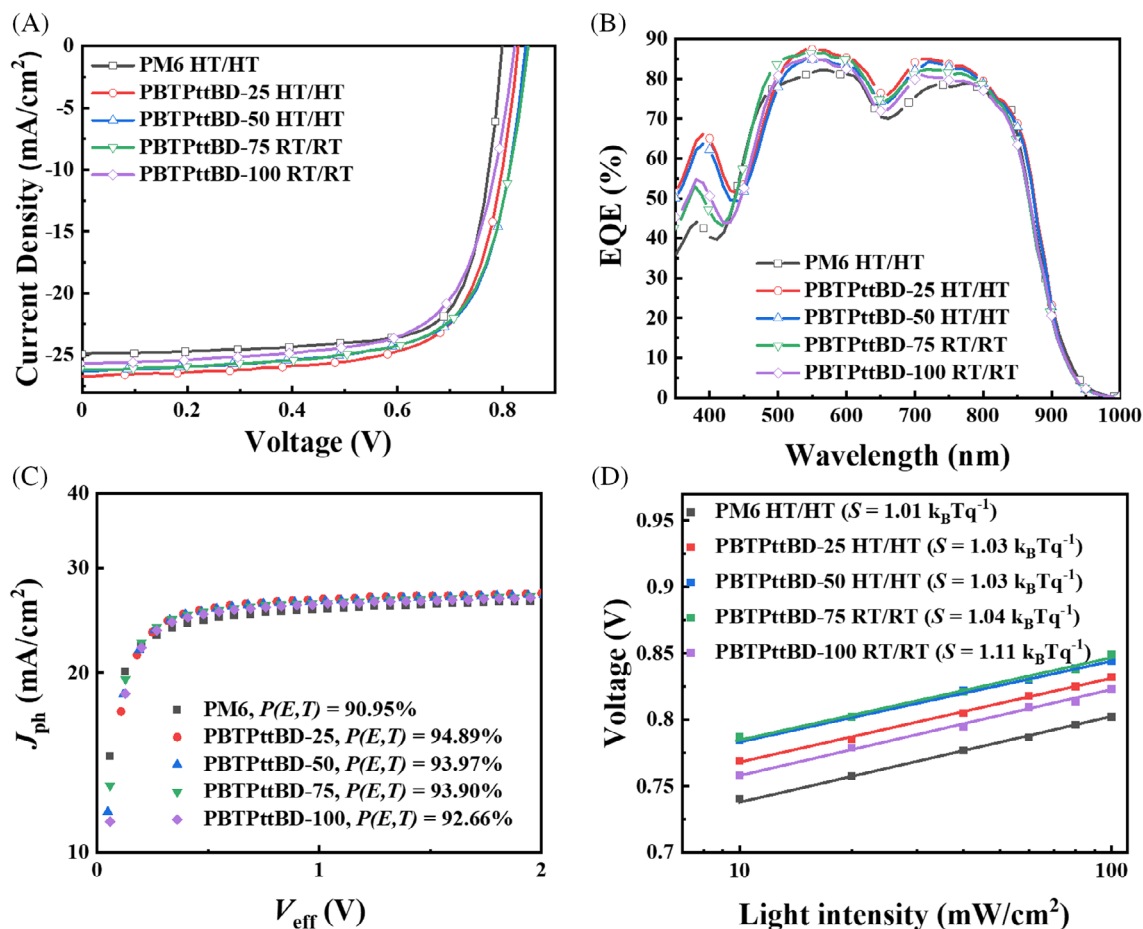
FIGURE 3 (A) Characteristic J-V curves under optimized conditions. (B) Corresponding external quantum efficiency curves of the HT-processed PM6:BTP-eC11, HT-processed PBTPttBD-25:BTP-eC11, HT-processed PBTPttBD-50:BTP-eC11, RT-processed PBTPttBD-75:BTP-eC11, and RT-processed PBTPttBD-100:BTP-eC11-based PSCs. (C) Measurement of photocurrent density (J_{ph}) versus effective voltage (V_{eff}) (D) V_{oc} versus light intensity.

TABLE 3 Solar cell performance of PM6:BTP-eC11 and PBTPttBD polymer:BTP-eC11-based PSCs under optimized processing conditions.

Polymer	Solution/ substrate [°C/°C]	V_{oc}[a][V]	J_{sc}[a][mA/cm²]	FF[a][%]	PCE[a][%]
PM6	80/80	0.80 (0.80 ± 0.01)	24.91 (24.78 ± 0.31)	75.57 (74.60 ± 1.35)	15.05 (14.85 ± 0.17)
PBTPttBD-25	80/80	0.83 (0.84 ± 0.01)	26.71 (26.42 ± 0.35)	71.21 (70.75 ± 0.37)	15.77 (15.65 ± 0.14)
PBTPttBD-50	80/80	0.84 (0.84 ± 0.01)	26.29 (26.26 ± 0.21)	70.55 (70.10 ± 0.69)	15.65 (15.46 ± 0.18)
PBTPttBD-75	25/25	0.85 (0.85 ± 0.01)	26.15 (26.02 ± 0.38)	70.05 (69.67 ± 0.95)	15.55 (15.32 ± 0.18)
PBTPttBD-100	25/25	0.82 (0.82 ± 0.01)	25.65 (25.80 ± 0.61)	69.33 (67.98 ± 1.52)	14.63 (14.42 ± 0.17)

[a]The average parameter values of 12 devices are presented in parentheses.

a higher PCE value than that achieved by the parent polymer (PM6 or PBTPttBD-100):BTP-eC11-based PSCs. This demonstrates that by introducing the appropriate content of TPD-TT component in the PM6 polymer backbone, high-performance PSCs processed with a nonhalogenated solvent can be successfully produced under RT processing conditions.

The external quantum efficiency (EQE) values of the PM6:BTP-eC11 and PBTPttBD polymer:BTP-eC11-based PSCs were measured to verify their photo response in the 350–1000 nm wavelength range (Figure 3B). The optical absorption spectra show that the polymer contributes to EQE in the short wavelength region (below 650 nm), whereas the BTP-eC11 contributes to EQE in the long

wavelength region (above 650 nm). Interestingly, the EQE values are slightly higher in the short wavelength region than those in the long wavelength region. This observation suggests that the photo-induced electron transfer pathway is relatively more efficient in generating charges than the hole transfer pathway.[42] On the other hand, the PBTPttBD polymer:BTP-eC11-based PSCs exhibited higher EQE values than those exhibited by PM6:BTP-eC11-based PSCs. This improvement can be attributed to the high absorption coefficient of the PBTPttBD polymers (Figure S3). Therefore, these results confirm that incorporating the TPD-TT component into the PM6 polymer backbone is an effective approach for achieving high J_{sc} and V_{oc} values.

To investigate the charge carrier dynamics of PM6:BTP-eC11 and PBTPttBD polymer:BTP-eC11-based PSCs, the maximum exciton generation rate (G_{max}) and exciton dissociation probability ($P(E,T)$) were measured using previously reported methods.[35,43-45] Figure 3C shows the dependence of photocurrent density (J_{ph}) on effective voltage (V_{eff}). The G_{max} value can be calculated from the equation of $J_{sat} = qG_{max}L$, where J_{sat} is the saturation current density at $V_{eff} = 2$ V, q is the electronic charge, and L is the thickness of active layer. The G_{max} was determined to be 1.50×10^{28} m^{-3} s^{-1} for PM6:BTP-eC11, 1.62×10^{28} m^{-3} s^{-1} for PBTPttBD-25:BTP-eC11, 1.61×10^{28} m^{-3} s^{-1} for PBTPttBD-50:BTP-eC11, 1.60×10^{28} m^{-3} s^{-1} for PBTPttBD-75:BTP-eC11, and 1.59×10^{28} m^{-3} s^{-1} for PBTPttBD-100:BTP-eC11. The high G_{max} value observed in the PBTTttBD terpolymer:BTP-eC11-based PSCs can be attributed to the higher absorption coefficient and broader absorption range of PBTTttBD terpolymer compared to PM6 polymer. Furthermore, the $P(E,T)$ is determined by the ratio of J_{ph}/J_{sat}. As shown in Figure 3C, the $P(E,T)$ of PM6:BTP-eC11, PBTPttBD-25:BTP-eC11, PBTPttBD-50:BTP-eC11, PBTPttBD-75:BTP-eC11, and PBTPttBD-100:BTP-eC11-based PSCs was found to be 90.95%, 94.89%, 93.97%, 93.90%, and 92.66%, respectively. In comparison to PM6:BTP-eC11-based PSCs, the PBTPttBD terpolymer:BTP-eC11-based PSCs exhibit relatively high $P(E,T)$ values exceeding 93%, indicating efficient exciton dissociation at the interface between PBTPttBD terpolymer and BTP-eC11. These results highlight that the superior G_{max} and $P(E,T)$ characteristics of the PBTPttBD terpolymer:BTP-eC11-based PSCs contributed to their higher J_{sc}.

We investigated the recombination properties of the fabricated PSCs by plotting V_{oc} as a function of light intensity (P_{light}). Figure 3D shows the logarithmic relation between V_{oc} and P_{light}, with a slope of kT/q. Here, k represents Boltzmann's constant, q is the elementary charge, and T denotes the temperature. When a monomolecular or a trap-assisted recombination process

occurs frequently in the photoactive layer, the slope (S) value tends to approach 2.[46,47] The corresponding slopes for PM6:BTP-eC11-based PSCs, PBTPttBD-25:BTP-eC11-based PSCs, PBTPttBD-50:BTP-eC11-based PSCs, PBTPttBD-75:BTP-eC11-based PSCs, and PBTPttBD-100:BTP-eC11-based PSCs are 1.01, 1.03, 1.03, 1.04, and 1.11 kT/q, respectively. Even with a 75% content of the TPD-TT component in the PBTPttBD polymer:BTP-eC11-based PSCs, the PSCs exhibited low slope values close to 1, suggesting a negligible monomolecular or trap-assisted recombination. However, the PBTPttBD-100:BTP-eC11-based PSC is susceptible to a frequent monomolecular or trap-assisted recombination, which explains its significantly lower FF compared to other PSCs.

To further understand the charge recombination behavior in the PM6:BTP-eC11 and PBTPttBD polymer:BTP-eC11-based PSCs, the P_{light} dependence of J_{sc} was examined. Figure S5 shows the double-logarithm diagram of the J_{sc} on the P_{light}. Typically, the power law relation between J_{sc} and P_{light} can be expressed as $J_{sc} \propto (P_{light})^{\alpha}$, where α is the recombination parameter. The value of α is associated with the bimolecular recombination in the photoactive layer and is close to 1, designating a low probability of bimolecular recombination.[48,49] The α values of PM6:BTP-eC11, PBTPttBD-25:BTP-eC11, PBTPttBD-50:BTP-eC11, PBTPttBD-75:BTP-eC11, and PBTPttBD-100:BTP-eC11-based PSCs were 0.98, 0.98, 0.97, 0.96, and 0.95, respectively, indicating that all PSCs exhibited negligible bimolecular recombination.

2.4 | Molecular ordering analysis

The crystallinity and structural properties of the polymers in the photoactive layers were examined by employing grazing incidence wide-angle x-ray scattering (GI-WAXS) analysis. The GI-WAXS images and diffraction peaks of the pristine polymer films are shown in Figure 4. A comprehensive overview of the packing parameters is presented in Table S2, along with the corresponding data obtained from the analysis. In the pristine polymer film, the PM6 exhibits clear and pronounced (h00) diffraction peaks at (100), (200), and (300) in the out-of-plane (OOP) direction, indicating a highly ordered packing structure and a prevailing edge-on orientation of the polymer. However, the intensity of (h00) peaks in the OOP direction is comparatively weaker in relation to the other polymer films, indicating reduced crystallinity, which is associated with the higher content of the TPD-TT component. In the pristine PBTPttBD polymer films, a more predominant face-on orientation with a π-π stacking (010) peak in the OOP direction and a lamella (100) peak in the in-plane direction is observed. Furthermore, by
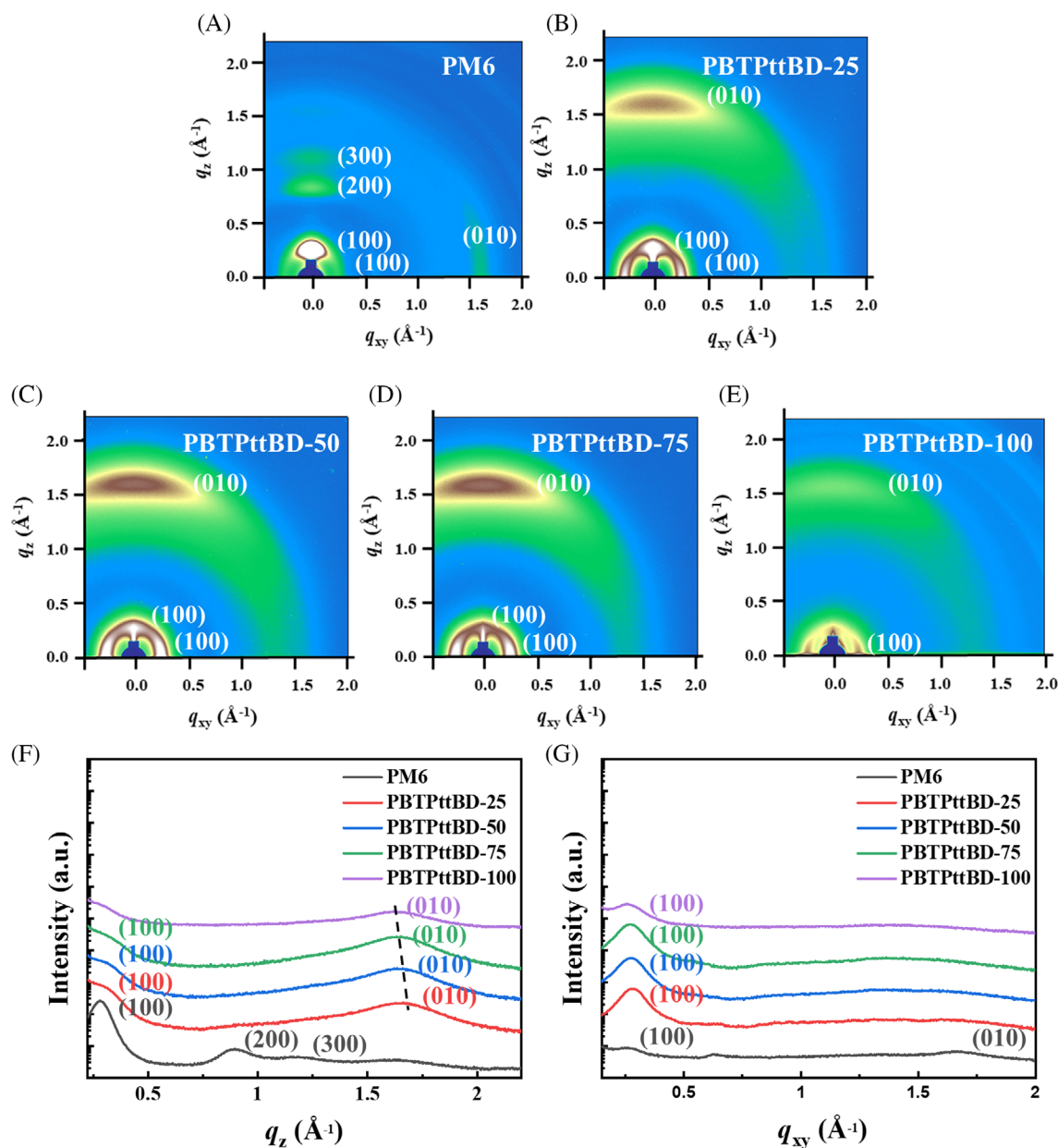
FIGURE 4   GI-WAXS images of (A) PM6, (B) PBTPttBD-25, (C) PBTPttBD-50, (D) PBTPttBD-75, and (E) PBTPttBD-100 pristine polymers. Line cut profiles of (F) out-of-plane and (G) in-plane of pristine polymers.

increasing the content of the TPD-TT component in the PM6 polymer backbone, a slight increase in the $\pi-\pi$ stacking distance from 3.78 to 3.85 Å is observed, indicating a weakened $\pi-\pi$ stacking interaction and structural disorder, which is the result of disrupted interchain interactions.

In contrast to the pristine polymer films, the molecular orientation of the PM6 and PBTPttBD-100 polymers is completely different when blended with the BTP-eC11, as shown in Figures S6 and S7. All blended films exhibit a prominent face-on orientation, which facilitates the efficient charge transport in the vertical direction. Table S3 shows an increased $\pi-\pi$ stacking distance in the OOP

direction and a decreased crystalline coherence length as the TPD-TT content in the PM6 polymer backbone increases. This result elucidates the decrease in FF, which is observed as the TPD-TT content in the PM6 polymer backbone increases. Furthermore, it is concluded that the excellent photovoltaic performance of PBTPttBD-75:BTP-eC11-based PSCs under RT processing can be attributed to their predominant face-on orientation, decreased crystallinity, and moderate $\pi-\pi$ stacking interactions.

Space-charge-limited current measurements were performed to evaluate the charge carrier mobilities of the PM6:BTP-eC11 and PBTPttBD polymer:BTP-eC11 blended
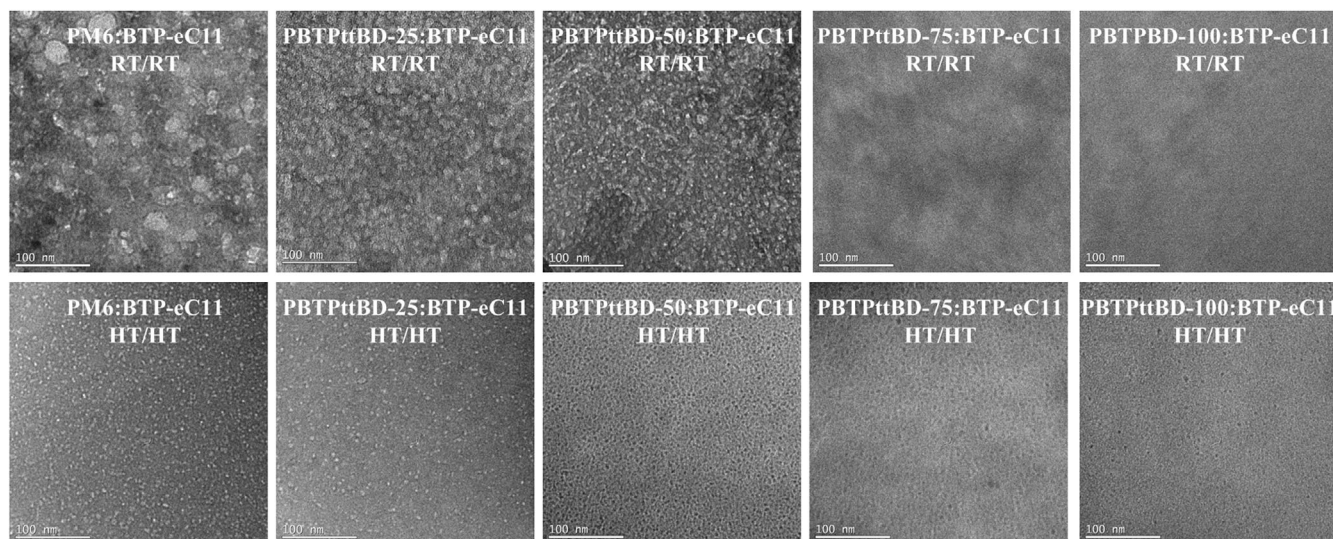
FIGURE 5 Transmission electron microscopy images of PM6:BPT-eC11 and PBTPttBD polymer:BTP-eC11 blended films under RT or HT processing conditions.

films. Figure S8 shows the *J-V* characteristics of the hole- and electron-only devices of PM6:BTP-eC11 and PBTPttBD polymer:BTP-eC11. The corresponding hole and electron mobilities are summarized in Table S4. The calculated hole mobility (μ_h) values for the PM6:BTP-eC11, PBTPttBD-25:BTP-eC11, PBTPttBD-50:BTP-eC11, PBTPttBD-75:BTP-eC11, and PBTPttBD-100:BTP-eC11 blended films were 2.92×10^{-4}, 2.72×10^{-4}, 2.54×10^{-4}, 2.48×10^{-4}, and 2.02×10^{-4} cm^2/V s, respectively. However, the electron mobility (μ_e) values of the PM6:BTP-eC11, PBTPttBD-25:BTP-eC11, PBTPttBD-50:BTP-eC11, PBTPttBD-75:BTP-eC11, and PBTPttBD-100:BTP-eC11 blended films were 2.60×10^{-4}, 3.20×10^{-4}, 3.05×10^{-4}, 3.35×10^{-4}, and 4.31×10^{-4} cm^2/V s, respectively. The corresponding μ_h/μ_e ratios were 1.12, 0.85, 0.83, 0.74, and 0.47. These values are consistent with the FF trend. The above results indicate that the PM6:BTP-eC11, PBTPttBD-25:BTP-eC11, PBTPttBD-50:BTP-eC11, and PBTPttBD-75:BTP-eC11 blended films exhibit nearly balanced electron-to-hole mobility (μ_e/μ_h) ratios, which contribute in achieving high FFs exceeding 70%.

2.5 | Surface morphological properties

Transmission electron microscopy images were obtained to investigate the effect of polymer backbone engineering and processing conditions on the morphology and phase separation of the photoactive layers. As shown in Figure 5, all polymer:BTP-eC11 blended films under HT processing conditions are homogeneous with a small domain size, without obvious phase separation. However,

the RT processed PM6:BTP-eC11, PBTPttBD-25:BTP-eC11, and PBTPttBD-50:BTP-eC11 blended films exhibit excessive molecular aggregation and rough film morphology, resulting in severe phase separation in the polymer/BTP-eC11 interfacial area. This is unfavorable to charge transport properties of the fabricated PSCs and may lead to a reduction in PCE. These results demonstrate why the RT processed PM6:BTP-eC11, PBTPttBD-25:BTP-eC11, and PBTPttBD-50:BTP-eC11-based PSCs exhibit much lower PCE values than those of the PBTPttBD-75:BTP-eC11-based PSCs.

Furthermore, the Flory-Huggins interaction parameter (χ) was measured to evaluate the miscibility between the polymer and BTP-eC11. Photographs of water and diiodomethane (DIM) droplets in each film are shown in Figure S9. The Flory-Huggins interaction parameters (χ) are summarized in Table S5. Achieving a balanced miscibility in photoactive films is critical for realizing high-performance PSCs. A low χ value indicates a high degree of miscibility in the photoactive films. However, the excessive miscibility can impede the exciton dissociation at the polymer-BTP-eC11 interface due to the homogeneous phase and a reduced interfacial area. Conversely, a high χ value results in a highly pure phase and a severe phase segregation, leading to an unfavorable morphology.[50,51] As shown in Table S5, the correlation between the composition of the TPD-TT component in the polymer backbone and χ value is evident. The PM6 film exhibits the highest χ value, indicating a weak interaction with the BTP-eC11. In contrast, the PBTPttBD-100 film exhibits the lowest χ value, which indicates its high miscibility with BTP-eC11. By increasing, the content of the TPD-TT component in the PBTPttBD polymers, the
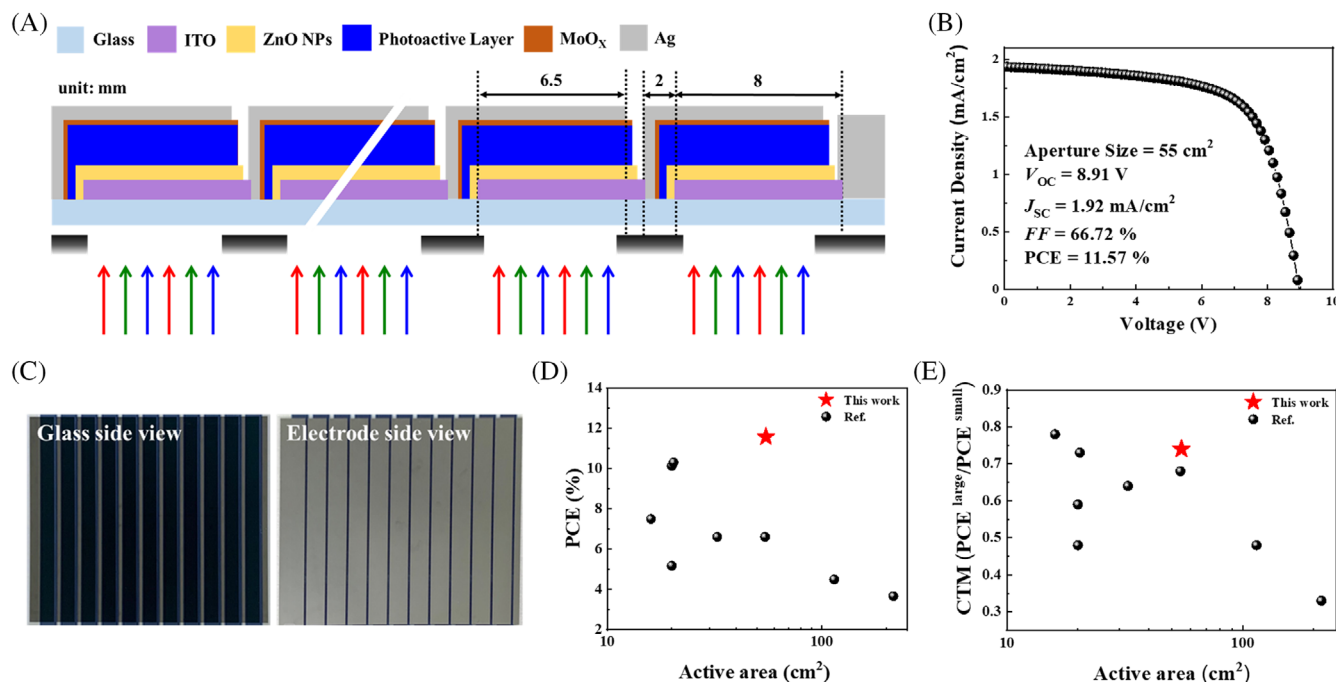
FIGURE 6 (A) Schematic of the PSC submodule fabrication design. (B) Best J-V curve of the PBTPttBD-75:BTP-eC11-based PSC submodules (C) Photograph of the PBTPttBD-75:BTP-eC11 PSC submodule using D-bar coating in air. (D) Plot of PCE values for large-area PSCs versus active area (> 10 cm²) in the nonhalogenated solvent systems. (E) Plot of CTM ratio for large-area PSCs versus active area (> 10 cm²) in nonhalogenated solvent systems.

intermolecular interaction and miscibility between the PBTPttBD polymers and BTP-eC11 is significantly improved, leading to the formation of a homogeneous film with a small domain size. Notably, the PBTPttBD-75 film exhibits a moderate χ value, resulting in a smooth and suitable phase separation, even when processed with nonhalogenated solvents under RT processing conditions. This result indicates that the incorporation of a certain content of the TPD-TT component into the PM6 polymer backbone promotes a favorable film morphology and enables mild processing conditions.

2.6 | PSC submodule performance

To demonstrate the compatibility of our PSC submodule design to commercialization and find a fitting solution for the scaling lag of large-area modules, we prepared a 10×10 cm² submodule comprised of 11 cells connected in series fashion with an active area of 55 cm², the schematic diagram is presented in Figure 6A. The D-bar coating of the ZnO and active layer was done under open-air conditions under 1-sun illumination, the best submodule with PBTPttBD-75:BTP-eC11 showed 11.57% efficiency owing to a high FF of 66.72%, J_{sc} of 1.92 mA/cm² and V_{oc} of 8.91 V and the corresponding J-V curve is shown in Figure 6B. Pictures of the glass and the electrode side of the PSC

submodule are presented in Figure 6C. The optimized submodule exhibited the minimal CTM loss, which can be attributed to the optimized crystallinity of the PBTPttBD-75:BTP-eC11 photoactive layer system and favorable film formation kinetics. The submodule also exhibited an excellent tolerance to device area variation during the transition from small to large-area module.[12] In general, the CTM loss appears during this transition process and can be primarily attributed to an increase in electrical losses caused by the ITO sheet resistance, geometrical losses introduced by increasing the cell width, and additional losses due to inhomogeneity and roughness of the active film. All these losses result in a suboptimal photovoltaic performance.[14] A plot of the PCE values versus active area is shown in Figure 6D. The PCE of PBTPttBD-75:BTP-eC11-based submodule is among the highest reported value using a nonhalogenated solvent over a 55 cm² active area module. Moreover, the PBTPttBD-75:BTP-eC11-based submodule exhibits an excellent CTM value of 0.74, which is among the highest reported for single-junction PSC submodules processed with nonhalogenated solvent (Figure 6E). Consequently, our findings provide a framework for additional investigation in the design of the terpolymers for RT and air processing conditions and present a roadmap for the smooth transition of small-scale devices to large-area modules, which are suitable for R2R processing and subsequent commercialization.

3 | CONCLUSION

In summary, we successfully synthesized a new series of 1D/2A terpolymers composed of BDT-F, TPD-TT, and BDD components for the development of RT and nonhalogenated solvent processed high-performance PSC submodules. Three PBTPttBD terpolymers, that is, PBTPttBD-25, PBTPttBD-50, and PBTPttBD-75, were synthesized by adjusting the ratios of the TPD-TT component to the BDD component to obtain TPD-TT contents of 25%, 50%, and 75%, respectively. The introduction of the TPD-TT component into the PM6 polymer backbone substantially improved the solubility in nonhalogenated solvents by decreasing the degree of structural order. Furthermore, the optical, electrochemical, charge-transport, nano-morphological properties of the PBTPttBD terpolymers was successfully modulated by adjusting the molar ratio of the TPD-TT and BDD components. GI-WAXS and contact angle analysis showed that the PBTPttBD-75: BTP-C11 blended film exhibits a predominant face-on orientation with good miscibility. As a result, the PBTPttBD-75:BTP-eC11 PSC, processed with *o*-xylene, achieved a high PCE value of 15.55%. Also, PBTPttBD-75: BTP-eC11-based PSC submodules, processed with *o*-xylene under RT conditions, achieved a notable PCE of 11.57% on a 55 cm² active area. This PCE value is among the highest reported using a nonhalogenated solvent over a 55 cm² active area module. In addition, the optimized submodule exhibited the minimal CTM loss, which can be attributed to the optimized crystallinity of the PBTPttBD-75:BTP-eC11 photoactive layer system and favorable film formation kinetics, demonstrating excellent tolerance to device area variation during the transition from small to large-area module. We anticipate that these results furnish a framework for additional investigation into the terpolymers strategy for RT and air processing and present a roadmap for the smooth transition of small-scale devices to large-area modules suitable for R2R processing and subsequent commercialization.

4 | EXPERIMENTAL SECTION

4.1 | General experimental information

PM6 and BTP-eC11 were prepared from Derthon and used without purification. BDD and BDT-F were purchased from Sunatech and used without further purification. All chemicals were obtained from Sigma-Aldrich and Alfa Aesar. TPD-TT monomer was synthesized following the reference.[35]

The elemental analysis of polymers was performed with elemental analyzers (Elementar). Thermogravimetric analysis of polymers was conducted using Auto TGA Q500 instrument. UV–vis absorption spectra of dilute polymer solutions and films were obtained by CARY 5000 spectrophotometer. CV measurements were performed by VMP3 and EC-Lab control software. TEM images were captured using NX10 instruments. GI-WAXS measurements were performed at PLS-II 9A U-SAXS beam line of Pohang Accelerator Laboratory (Republic of Korea). Hole and electron mobilities of PM6:BTP-eC11 and PBTPttBD polymer:BTP-eC11 blended films were obtained by space charge limited current (SCLC) method using device structures of indium tin oxide (ITO)/poly(3,-4-ethylenedioxythiophene):poly(styrene sulfonate) (PEDOT:PSS)/PM6:BTP-eC11 and PBTPttBD polymer:BTP-eC11/Au (holy-only) and ITO/ZnO/PM6:BTP-eC11 and PBTPttBD polymer:BTP-eC11/LiF/Al (electron-only). The γ values of the polymer films were obtained from the Wu model. The calculation of Flory-Huggins interaction parameter (χ) follows the methodology established in a previous study.[33]

4.2 | Synthesis

4.2.1 | For the polymerization of PBTPttBD-25

In a double-neck round-bottom flask (10 mL), BDT-F (132 mg, 0.138 mmol), BDD (80 mg, 0.103 mmol), TPD-TT (36 mg, 0.035 mmol), P(*o*-tolyl)₃ (3.36 mg, 0.011 mmol), and Pd₂(dba)₃ (2.53 mg, 0.003 mmol) were combined in anhydrous chlorobenzene (3 mL). The mixture was degassed under nitrogen for 20 min and then refluxed for 72 h. The resulting polymers were purified in a Soxhlet extractor using sequential solvents: methanol, *n*-hexane, and dichloromethane. The undissolved polymer was further extracted with CF. After that, condensed under reduced pressure, reprecipitated in methanol (80 mL) and dried under vacuum for 24 h. PBTPttBD-25 was obtained as shiny black material. Elemental analysis calculated: C = 67.18%, H = 6.56%, N = 0.27%, S = 20.55%. Found: C = 66.15%, H = 6.67%, N = 0.26%, S = 19.52%.

4.2.2 | For the polymerization of PBTPttBD-50

In a double-neck round-bottom flask (10 mL), BDT-F (132 mg, 0.138 mmol), BDD (53 mg, 0.069 mmol), TPD-TT (71 mg, 0.069 mmol), P(*o*-tolyl)₃ (3.36 mg, 0.011 mmol), and Pd₂(dba)₃ (2.53 mg, 0.003 mmol) were combined in anhydrous chlorobenzene (3 mL). The

mixture was degassed under nitrogen for 20 min and then refluxed for 72 h. The resulting polymers were purified in a Soxhlet extractor using sequential solvents: methanol, *n*-hexane, and dichloromethane. The undissolved polymer was further extracted with CF. After that, condensed under reduced pressure, reprecipitated in methanol (80 mL) and dried under vacuum for 24 h. PBTPttBD-50 was obtained as shiny black material. Elemental analysis calculated: C = 67.39%, H = 6.81%, N = 0.52%, S = 20.12%. Found: C = 67.18%, H = 7.07%, N = 0.49%, S = 19.72%.

4.2.3 | For the polymerization of PBTPttBD-75

In a double-neck round-bottom flask (10 mL), BDT-F (132 mg, 0.138 mmol), BDD (26 mg, 0.0345 mmol), TPD-TT (107 mg, 0.104 mmol), P(*o*-tolyl)$_3$ (3.36 mg, 0.011 mmol), and Pd$_2$(dba)$_3$ (2.53 mg, 0.003 mmol) were combined in anhydrous chlorobenzene (3 mL). The mixture was degassed under nitrogen for 20 min and then refluxed for 72 h. The resulting polymers were purified in a Soxhlet extractor using sequential solvents: methanol, *n*-hexane, and dichloromethane. The undissolved polymer was further extracted with CF. After that, condensed under reduced pressure, reprecipitated in methanol (80 mL) and dried under vacuum for 24 h. PBTPttBD-75 was obtained as shiny black material. Elemental analysis calculated: C = 67.57%, H = 7.04%, N = 0.74%, S = 19.73%. Found: C = 67.35%, H = 7.14%, N = 0.72%, S = 19.55%.

4.2.4 | For the polymerization of PBTPttBD-100

In a double-neck round-bottom flask (10 mL), BDT-F (132 mg, 0.138 mmol), TPD-TT (143 mg, 0.138 mmol), P(*o*-tolyl)$_3$ (3.36 mg, 0.011 mmol), and Pd$_2$(dba)$_3$ (2.53 mg, 0.003 mmol) were combined in anhydrous chlorobenzene (3 mL). The mixture was degassed under nitrogen for 20 min and then refluxed for 72 h. The resulting polymers were purified in a Soxhlet extractor using sequential solvents: methanol, *n*-hexane, and dichloromethane. The undissolved polymer was further extracted with CF. After that, condensed under reduced pressure, reprecipitated in methanol (80 mL) and dried under vacuum for 24 h. PBTPttBD-100 was obtained as shiny black material. Elemental analysis calculated: C = 67.74%, H = 7.24%, N = 0.94%, S = 19.38%. Found: C = 67.25%, H = 7.42%, N = 0.92%, S = 19.11%.

4.3 | Device fabrication

4.3.1 | Small-area PSCs fabrication

Device structures were fabricated with the structure of ITO/ZnO/PM6:BTP-eC11 and PBTPttBD polymer:BTP-eC11/MoO$_3$/Ag. The ITO-coated glass substrates were treated by ultrasonication with acetone, water, and isopropyl alcohol for 15 min. Then, the ITO substrates were dried for 50 min in an oven (60°C), and then UV-ozone treated for 30 min. Spin-coating of the ZnO solution was performed at 3000 rpm onto the ITO substrates. Then, the film/substrate was annealed in the air for 10 min at 120°C. All subsequent steps were carried out in a glove box under N$_2$ atmosphere. For the active solutions, polymer:BTP-eC11 (1:1.5, 16 mg/mL) with 1,8-diiodooctane (0.5 v/v%) was dissolved together in *o*-xylene overnight. The HT process proceeded as follows: Prior to spin-coating, both the substrates and the polymer:BTP-eC11 blend solution was transferred to a controlled environment inside a glove box. Inside the glove box, the blend solution was heated to 80°C, while the substrate was also preheated to the same temperature of 80°C, ensuring optimal conditions for the subsequent spin-coating process. On the other hand, the RT process proceeded as follows: substrates and solution were stirred constantly at RT, and the photoactive films were spin-coated for 40 s. Afterward, the active solution was spin-coated onto the ZnO/ITO substrate to form an active layer. The samples were annealed at 100°C for 10 min. Following that, a sequential deposition of a 10 nm thick MoO$_3$ layer and a 100 nm thick Ag layer was performed onto the active layer.

The *J-V* characteristics of the devices were then measured under standard one sun conditions, specifically AM 1.5G with an intensity of 100 mW/cm^2. All devices utilized in the measurements had an active area of 0.05 cm^2.

4.3.2 | Large-area PSC sub-modules fabrication

The fabrication of the PSC sub-module involved employing a bar-coating technique, with the D-bar coater being acquired from PEMS (Printed Electro-Mechanical System, South Korea). Inverted device structures were used to fabricate BHJ-PSCs with the following configurations: ITO/ZnO/PBTPttBD-75:BTP-eC11/MoO$_3$/Ag. After a 30-min UV-ozone treatment, a solution of ZnO nanoparticles were coated by solution shearing on the prepatterned sub-module substrate (gap: 100 μm, coating speed: 5 mm/s) and annealed at 120°C for 15 min. Active materials were coated by solution shearing (gap: 100 μm, coating speed: 5 mm/s) and annealed at 100°C for

10 min. Following that, a sequential deposition of a 10 nm thick MoO_3 layer and a 100 nm thick Ag layer was evaporated under base pressure of 1.6×10^{-6} torr. The J-V characteristics of the devices were then measured under standard one sun conditions, specifically AM 1.5G with an intensity of 100 mW/cm^2. Determining the sub-module area using an aperture with an area smaller than the overlap of the top and bottom electrodes will improve accuracy when evaluating photovoltaic performance. It is worth noting that PSC sub-module utilized in the measurements had an active area of 55 cm^2.

AUTHOR CONTRIBUTIONS

Hyeonwoo Jung: Experimentation, methodology, validation, writing – original draft. **Jongyoun Kim:** Experimentation, formal analysis. **Jaehyoung Park:** Experimentation, methodology. **Muhammad Jahankhan:** Experimentation, methodology. **Youngjun Hwang:** Experimentation, data curation. **Byeongjae Kang:** Experimentation, data curation. **Hyerin Kim:** Experimentation, data curation. **Ho-Yeol Park:** Methodology, formal analysis. **Pyeongkang Ahn:** Experimentation. **DuHyeon Um:** Experimentation. **Je-Sung Jee:** Formal analysis. **Won Suk Shin:** Formal analysis. **Bong-Soo Kim:** Formal analysis. **Sung-Ho Jin:** Methodology, project administration, supervision, writing – review & editing. **Chang Eun Song:** Validation, project administration, supervision, writing – review & editing. **Youngu Lee:** Conceptualization, validation, project administration, supervision, writing – review & editing.

ACKNOWLEDGMENTS

CONFLICT OF INTEREST STATEMENT

The authors declare no conflict of interest.

ORCID

Hyeonwoo Jung https://orcid.org/0000-0003-0962-6280
Youngu Lee https://orcid.org/0000-0001-5014-1117

REFERENCES

1. Zhang G, Zhao J, Chow P, et al. Nonfullerene acceptor molecules for bulk heterojunction organic solar cells. *Chem Rev.* 2018;118(7):3447-3507. doi:10.1021/acs.chemrev.7b00535

2. Lee C, Lee S, Kim G-U, Lee W, Kim B. Recent advances, design guidelines, and prospects of all-polymer solar cells. *Chem Rev.* 2019;119(13):8028-8086. doi:10.1021/acs.chemrev.9b00044

3. Fu H, Li Y, Yu J, et al. High efficiency (15.8%) all-polymer solar cells enabled by a regioregular narrow bandgap polymer acceptor. *J Am Chem Soc.* 2021;143(7):2665-2670. doi:10.1021/jacs.0c12527

4. Meng L, Zhang Y, Wan X, et al. Organic and solution-processed tandem solar cells with 17.3% efficiency. *Science.* 2018;361(6407):1094-1098. doi:10.1126/science.aat2612

5. Jiang K, Zhang J, Zhong C, et al. Suppressed recombination loss in organic photovoltaics adopting a planar–mixed hetero-junction architecture. *Nat Energy.* 2022;7(11):1076-1086. doi:10.1038/s41560-022-01138-y

6. Zhu L, Zhang M, Xu J, et al. Single-junction organic solar cells with over 19% efficiency enabled by a refined double-fibril network morphology. *Nat Mater.* 2022;21(6):656-663. doi:10.1038/s41563-022-01244-y

7. Han C, Wang J, Zhang S, et al. Over 19% efficiency organic solar cells by regulating multidimensional intermolecular interactions. *Adv Mater.* 2023;35(10):2208986. doi:10.1002/adma.202208986

8. Cui Y, Xu Y, Yao H, et al. Single-junction organic photovoltaic cell with 19% efficiency. *Adv Mater.* 2021;33(41):2102420. doi:10.1002/adma.202102420

9. Lv J, Tang H, Huang J, et al. Additive-induced miscibility regulation and hierarchical morphology enable 17.5% binary organic solar cells. *Energy. Environ Sci.* 2021;14(5):3044-3052. doi:10.1039/d0ee04012f

10. Sun G, Jiang X, Li X, et al. High performance polymerized small molecule acceptor by synergistic optimization on π-bridge linker and side chain. *Nat Commun.* 2022;13(1):5267. doi:10.1038/s41467-022-32964-z

11. Park S, Park S, Kurniawan D, Son J, et al. Highly efficient large-area organic photovoltaic module with a 350 nm thick active layer using a random terpolymer donor. *Chem Mater.* 2020;32(8):3469-3479. doi:10.1021/acs.chemmater.9b05399

12. Sun R, Wu Q, Guo J, et al. A layer-by-layer architecture for printable organic solar cells overcoming the scaling lag of module efficiency. *Joule.* 2020;4(2):407-419. doi:10.1016/j.joule.2019.12.004

13. Ghasemi M, Balar N, Peng Z, et al. A molecular interaction–diffusion framework for predicting organic solar cell stability. *Nat Mater.* 2021;20(4):525-532. doi:10.1038/s41563-020-00872-6

14. Yoon S, Park S, Park S, et al. High-performance scalable organic photovoltaics with high thickness tolerance from 1 cm^2 to above 50 cm^2. *Joule.* 2022;6(10):2406-2422. doi:10.1016/j.joule.2022.07.014

15. Du B, Ma Y, Guo C, et al. Hot-casting boosts efficiency of halogen-free solvent processed non-fullerene organic solar cells. *Adv Funct Mater.* 2021;31(45):2105794. doi:10.1002/adfm.202105794

16. Dong S, Jia T, Zhang K, Jing J, Huang F. Single-component non-halogen solvent-processed high-performance organic solar cell module with efficiency over 14%. *Joule.* 2020;4(9):2004-2016. doi:10.1016/j.joule.2020.07.028

17. Chen J, Cao J, Liu L, et al. Layer-by-layer processed PM6:Y6-based stable ternary polymer solar cells with improved efficiency over 18% by incorporating an asymmetric thieno[3,2-b]indole-based acceptor. *Adv Funct Mater.* 2022;32(25):2200629. doi:10.1002/adfm.202200629

18. Jiang K, Zhang J, Peng Z, et al. Pseudo-bilayer architecture enables high-performance organic solar cells with enhanced exciton diffusion length. *Nat Commun*. 2021;12(1):468. doi:10.1038/s41467-020-20791-z

19. Yan C, Ma R, Cai G, et al. Reducing V_{OC} loss via structure compatible and high lowest unoccupied molecular orbital nonfullerene acceptors for over 17%-efficiency ternary organic photovoltaics. *EcoMat*. 2020;2(4):e12061. doi:10.1002/eom2.12061

20. Jung H, Yu G, Jang S, et al. High-performance polymer solar cells based on terpolymer composed of one donor and two acceptors processed with non-halogenated solvent. *Org Electron*. 2020;86:105929. doi:10.1016/j.orgel.2020.105929

21. Wu Q, Yu Y, Xia X, et al. High-performance organic photovoltaic modules using eco-friendly solvents for various indoor application scenarios. *Joule*. 2022;6(9):2138-2151. doi:10.1016/j.joule.2022.07.001

22. Heo H, Kim H, Lee D, et al. Regioregular D$_1$-A-D$_2$-A terpolymer with controlled thieno[3,4-*b*]thiophene orientation for high-efficiency polymer solar cells processed with nonhalogenated solvents. *Macromolecules*. 2016;49(9):3328-3335. doi:10.1021/acs.macromol.6b00269

23. Cui Y, Yao H, Hong L, et al. Achieving over 15% efficiency in organic photovoltaic cells via copolymer design. *Adv Mater*. 2019;31(14):1808356. doi:10.1002/adma.201808356

24. Jung H, Kim H, Kim J, Jang S, Lee Y. Side-chain engineering of regioregular copolymers for high-performance polymer solar cells processed with nonhalogenated solvents. *Bull Korean Chem Soc*. 2022;43(10):1200-1206. doi:10.1002/bkcs.12606

25. Xu X, Yu L, Yan H, Li R, Peng Q. Highly efficient non-fullerene organic solar cells enabled by a delayed processing method using a non-halogenated solvent. *Energ Environ Sci*. 2020;13(11):4381-4388. doi:10.1039/d0ee02034f

26. Liu B, Sun H, Lee J-W, et al. Achieving highly efficient all-polymer solar cells by green-solvent-processing under ambient atmosphere. *Energ Environ Sci*. 2021;14(8):4499-4507. doi:10.1039/d1ee01310f

27. Lee J-W, Lim C, Lee S-W, et al. Intrinsically stretchable and non-halogenated solvent processed polymer solar cells enabled by hydrophilic spacer-incorporated polymers. *Adv Energy Mater*. 2022;12(46):2202224. doi:10.1002/aenm.202202224

28. Rehman Z, Haris M, Ryu S, et al. Trifluoromethyl-substituted conjugated random terpolymers enable high-performance small and large-area organic solar cells using halogen-free solvent. *Adv Sci*. 2023;10(21):2302376. doi:10.1002/advs.202302376

29. Li Y, Liu H, Wu J, et al. Additive and high-temperature processing boost the photovoltaic performance of nonfullerene organic solar cells fabricated with blade coating and nonhalogenated solvents. *ACS Appl Mater Interfaces*. 2021;13(8):10239-10248. doi:10.1021/acsami.0c23035

30. Wu J, Li G, Fang J, et al. Random terpolymer based on thiophene-thiazolothiazole unit enabling efficient nonfullerene organic solar cells. *Nat Commun*. 2020;11(1):4612. doi:10.1038/s41467-020-18378-9

31. Heo H, Kim H, Nam G, Lee D, Lee Y. Multi-donor random terpolymers based on benzodithiophene and dithienosilole

32. Liao Z, Hu D, Tang H, et al. 18.42% efficiency polymer solar cells enabled by terpolymer donors with optimal miscibility and energy levels. *J Mater Chem A*. 2022;10(14):7878-7887. doi:10.1039/d1ta10644a

33. Jung H, Yu G, Kim J, et al. Unprecedented long-term thermal stability of 1D/2A terpolymer-based polymer solar cells processed with nonhalogenated solvent. *Sol RRL*. 2021;5(11):2100513. doi:10.1002/solr.202100513

34. Ha J-W, Jung J, Ryu D, et al. Thienoquinolinone-based acceptor-π-acceptor-type building block for polymer donors in organic solar cells. *Macromol Res*. 2023;31(1):25-31. doi:10.1007/s13233-023-00112-1

35. Park J, Kim G-U, Lee D, et al. Importance of optimal crystallinity and hole mobility of BDT-based polymer donor for simultaneous enhancements of V_{oc}, J_{sc}, and FF in efficient nonfullerene organic solar cells. *Adv Funct Mater*. 2020;30(51):2005787. doi:10.1002/adfm.202005787

36. Ha J-W, Song C, Kim H, Ryu D, Shin W, Hwang D-H. Highly efficient and photostable ternary organic solar cells enabled by the combination of non-fullerene and fullerene acceptors with thienopyrrolodione-based polymer donors. *ACS Appl Mater Interfaces*. 2020;12(46):51699-51708. doi:10.1021/acsami.0c14367

37. Chau H, Kataria M, Kwon N, et al. Improved photovoltaic performance of ternary all-polymer solar cells by incorporating a new Y6-based polymer acceptor and PC$_{61}$BM. *Macromol Res*. 2022;30(8):587-596. doi:10.1007/s13233-022-0069-x

38. Kim J, Park J, Song D, et al. BDT-based donor polymer for organic solar cells to achieve high efficiency over 15% for ternary organic solar cells. *Macromol Res*. 2023;31(5):489-497. doi:10.1007/s13233-023-00117-w

39. Kim H, Lee H, Seo D, et al. Regioregular low bandgap polymer with controlled thieno[3,4-*b*]thiophene orientation for high-efficiency polymer solar cells. *Chem Mater*. 2015;27(8):3102-3107. doi:10.1021/acs.chemmater.5b00632

40. Rasool S, Vu D, Song C, et al. Room temperature processed highly efficient large-area polymer solar cells achieved with molecular engineering of copolymers. *Adv Energy Mater*. 2019;9(21):1900168. doi:10.1002/aenm.201900168

41. Ma L, Zhang S, Yao H, et al. High-efficiency nonfullerene organic solar cells enabled by 1000 nm thick active layers with a low trap-state density. *ACS Appl Mater Interfaces*. 2020;12(16):18777-18784. doi:10.1021/acsami.0c05172

42. Wen S, Li Y, Zheng N, Raji I, Yang C, Bao X. High-efficiency organic solar cells enabled by halogenation of polymers based on 2D conjugated benzobis(thiazole). *J Mater Chem A*. 2020;8(27):13671-13678. doi:10.1039/d0ta04734a

43. Kim J, Kim G-U, Kim D, et al. Development of rigidity-controlled terpolymer donors for high-performance and mechanically robust organic solar cells. *J Mater Chem A*. 2023;11(9):4808-4817. doi:10.1039/d2ta09990j

44. Rasool S, Kim J, Cho H, et al. Morphologically controlled efficient air-processed organic solar cells from halogen-free solvent system. *Adv Energy Mater*. 2023;13(7):2203452. doi:10.1002/aenm.202203452

segments with different monomer compositions for high-performance polymer solar cells. *Macromol Res*. 2018;26(3):238-245. doi:10.1007/s13233-018-6030-3

45. Lee J, Bae S, Jo W. Synthesis of 6H-benzo[c]chromene as a new electron-rich building block of conjugated alternating copolymers and its application to polymer solar cells. *J Mater Chem A*. 2014;2(34):14146-14153. doi:10.1039/c4ta02929a

46. Kim H, Lim B, Heo H, et al. High-efficiency organic photovoltaics with two-dimensional conjugated benzodithiophene-based regioregular polymers. *Chem Mater*. 2017;29(10):4301-4310. doi:10.1021/acs.chemmater.7b00595

47. Lee Y, Yeop J, Kim J, Woo HY. Fullerene-based photoactive A-D-A triads for single-component organic solar cells: Incorporation of non-fused planar conjugated core. *Macromol Res*. 2021;29(12):871-881. doi:10.1007/s13233-021-9100-x

48. Park S, Ahn J-S, Kwon N, et al. Effect of fused thiophene bridges on the efficiency of non-fullerene polymer solar cells made with conjugated donor copolymers containing alkyl thiophene-3-carboxylate. *Macromol Res*. 2021;29(6):435-442. doi:10.1007/s13233-021-9053-0

49. Salma S, Kim J. Effect of the side chain functionality of the conjugated polyelectrolytes as a cathode interlayer material on the photovoltaic performances. *Macromol Res*. 2022;30(2):146-151. doi:10.1007/s13233-022-0011-2

50. Kranthiraja K, Kim H, Lee J, et al. Side chain functionalization of conjugated polymer on the modulation of photovoltaic properties of fullerene and non-fullerene organic solar cells. *Macromol Res*. 2023;31(9):897-905. doi:10.1007/s13233-023-00176-z

51. Du J, Hu K, Zhang J, et al. Polymerized small molecular acceptor based all polymer solar cells with an efficiency of 16.16% via tuning polymer blend morphology by molecular design. *Nat commun*. 2021;12:5264. doi:10.1038/s41467-021-25638-9

SUPPORTING INFORMATION

Additional supporting information can be found online in the Supporting Information section at the end of this article.